Journal of Membrane Science 641 (2022) 119928

Contents lists available at ScienceDirect

Journal of Membrane Science

journal homepage: www.elsevier.com/locate/memsci

CO_2-responsive membranes prepared by selective swelling of block copolymers and their behaviors in protein ultrafiltration

Chenxu Zhang, Jiemei Zhou **, Xiangyue Ye, Zhuo Li, Yong Wang *

State Key Laboratory of Materials-Oriented Chemical Engineering, College of Chemical Engineering, Nanjing Tech University, Nanjing, 211816, Jiangsu, PR China

ARTICLE INFO

Keywords:
CO_2 switchability
Block copolymer
Selective swelling
Protein ultrafiltration
Responsive membranes

ABSTRACT

Due to the predominance of CO_2 as a new trigger with source abundance, non-toxicity, good reversibility and no byproduct accumulation compared to other triggers, CO_2-responsive membranes recently attract wide interest in stimuli-switchable separation. Here we report on the development of CO_2-responsive nanoporous membranes with poly(2-dimethylaminoethyl methacrylate)-*block*-polystyrene (PDMAEMA-*b*-PS) block polymer (BCP) under the instruction of selective swelling-induced pore generation strategy, where hydrophilic chains of PDMAEMA can be enriched on the membrane surface and pore walls in the swelling process. The tertiary amine of PDMAEMA can be reversibly switched in conformation and charge property under the stimulation of CO_2/N_2. The CO_2-responsive behavior of PDMAEMA enriched on the surface and pore walls has further enabled as-prepared membranes to feature the tunable pore size by introducing and removing CO_2 gas. As a result, the PDMAEMA-*b*-PS nanoporous membranes exhibit excellent regulation in separation performances in terms of the permeance and rejection to varied proteins under the stimulation of CO_2/N_2. This work represents a simple and reliable way for making CO_2-responsive membranes.

1. Introduction

As the typical membrane-based separation process, ultrafiltration can effectively realize high purity separation in removing biological macromolecules and colloid particles [1,2]. Ultrafiltration process depends mainly on size sieving as separation principle and pressure decline as driving force, meanwhile, surface properties of ultrafiltration membranes also determine the performance [3,4]. Conventional membranes often have invariable pore sizes and surface properties, which restrains their potential applications in versatile fields such as controlled release, biosensing and smart separation due to the absence of stimuli-responsiveness [5]. Hence, to incorporate chemically/physically stimuli-responsive materials to the membranes is in demand, so as to make membranes switchable in pore sizes and surface properties [6], thus, the corresponding separation performances including the permeability and selectivity could be regulated under the stimulation of external environment.

The stimuli-responsive membranes in response to various stimuli sources containing temperature [7], light [8], magnetic field [9], pH [10], ionic strength [11], etc. have been developed during the past decades. Among them, gas-responsive membranes show particular advantages on account of simply adding and removing stimulus by bubbling stimuli and inert gas alternatively. Especially, CO_2-responsive membranes with artificial smart pore gates applied in separation field have caused broad concerns in recent years [12,13]. For one thing, CO_2 as the trigger offers prominent advantages of abundant, cost-effective and nontoxic. For another, the adding and removing of CO_2 occur under mild conditions and without byproduct accumulation [14]. Yuan et al. [15]. prepared smart nanostructured membranes for oil/water separation by electrospinning of polymethylmethacrylate–*co*-poly (N, N-diethylaminoethyl methacrylate) (PMMA-*co*-PDEAEMA) polymer. The membranes exhibited reversible regulation on surface oil/water wettability due to the presence of CO_2-responsive polymer of PDEAEMA, thus controlled oil/water separation could be realized under the stimulation of CO_2. Zhao et al. [16]. reported CO_2-responsive membranes by grafting PDEAEMA on the pore surface of polyvinylidene fluoride (PVDF) membranes coated with a polydopamine layer *via* Michael addition, in which the permeance and rejection to Au nanoparticles could be easily regulated under the stimulation of CO_2.

For the preparation of CO_2-responsive membranes, introducing CO_2-

* Corresponding author.
** Corresponding author.
E-mail addresses: zhoujm@njtech.edu.cn (J. Zhou), yongwang@njtech.edu.cn (Y. Wang).

https://doi.org/10.1016/j.memsci.2021.119928
Received 15 August 2021; Received in revised form 17 September 2021; Accepted 24 September 2021
Available online 1 October 2021

responsive groups into membranes is necessary. Physical blending and chemical grafting are always used in membranes fabrication [17–19]. Particularly, chemical grafting has been proved to be the most used and effective way to introduce stimuli-responsive groups, which can ensure stable under the long-term usage [20]. However, chemical grafting also faces some challenging problems inevitably, such as complex treatment, difficult enlargement [21] and so on. Our group recently develop a nondestructive strategy of selective swelling-induced pore generation for preparing nanoporous membranes with block copolymers (BCPs) served as membrane-forming materials. Microdomains of the minority blocks can experience volume expansion and chains migration by immersing the dense BCP films into the swelling bath, followed by chains collapse to form interconnected nanoporous structures after air drying, which enable as-prepared membranes to feature permanent surface functionality and stimuli-responsiveness [22]. Ultrafiltration membranes with poly(2-vinylpyridine) chains coated on surface and pore walls were prepared by using this strategy in our previous studies, and related pH-responsive property for regulating permeability was also reported [23–26]. Based on previous discoveries and understandings, in this study, we developed CO_2-responsive membranes with poly (2-dimethylaminoethyl methacrylate)-*block*-polystyrene (PDMAEMA-*b*-PS) BCP served as the membrane-forming material by the process of selective swelling-induced pore generation. PDMAEMA, as one block of BCP material, is a representative CO_2-responsive polymer. It is near-neutral with a pKa value of 7 while would be protonated in the presence of CO_2 because of the reaction between tertiary amine groups with CO_2 in water [27,28]. We first immersed PDMAEMA-*b*-PS dense films in hot ethanol to generate pores and simultaneously to enrich the PDMAEMA blocks onto the membrane surface and pore walls. The surface-enriched PDMAEMA chains render thus-prepared membranes the capability to switch both pore size and surface charging under the stimulation of CO_2 exposure and elimination. The CO_2 switchability of the membranes was then utilized to effectively manipulate the ultrafiltration performances.

2. Experimental section

2.1. Materials

PDMAEMA-*b*-PS block copolymer ($M_n^{PDMAEMA}$ = 20.8 kDa, M_n^{PS} = 60 kDa, PDI = 1.26) was synthesized according to our previous work [29]. Silicon wafer was treated by ultrasonic cleaning before using. PVDF membranes with a mean pore diameter of 220 nm were purchased from Millipore and used as microfiltration substrates. Bovine serum albumin (BSA, M_w = 66 kDa) was purchased from MP Biomedicals, Ltd. Bovine hemoglobin (BHb, M_w = 64.5 kDa) was obtained from Shanghai yuanye Bio-Technology Co., Ltd. Lysozyme (M_w = 14.3 kDa) and cytochrome *c* (M_w = 12.4 kDa) were purchased from Sigma-Aldric. Chloroform (≥99%), ethanol (≥99.7%), tetrahydrofuran (≥99.5%) and methanol (≥99%) were provided by local suppliers and used as received without further purification. Deionized water (8–20 μS/cm) was used throughout this work.

2.2. Micelles preparation

PDMAEMA-*b*-PS (10 mg) was dissolved in THF (1 mL). Subsequently, deionized water (9 mL) was slowly added under vigorously stirring treatment followed by stirring for 5 h. Then THF was removed by dialysis (cutoff = 8–14 kDa) against deionized water for 24 h to obtain the BCP micellar solution.

2.3. Preparation of PDMAEMA-b-PS thin films

PDMAEMA-*b*-PS was dissolved in chloroform to prepare the film-forming solution with a concentration of 2 wt%. The solution was repeatedly filtrated through PTFE filters three times to remove any impurities. Subsequently, the BCP solution was spin-coated on cleaned silicon wafers at 2000 rpm for 30 s. As-prepared films were dried at 60 °C for 20 min to evaporate the residual solvent. Then, the films were soaked in ethanol at 65 °C to perform selective swelling-induced pore generation. After preset durations, the films were withdrawn from ethanol and dried naturally.

2.4. Preparation of PDMAEMA-b-PS membranes

Briefly, PVDF macroporous substrates were immersed in deionized water for 30 min to fill the pores with water, which can prevent the BCP solution from downward leaking in the process of spin coating. Subsequently, PVDF substrates were attached on glass slides followed by wiping out redundant water on the substrate surface. The BCP solution was then spin-coated on PVDF substrates at 2000 rpm for 30 s, followed by drying at 65 °C for 20 min to evaporate organic solvent and residual water. Selective swelling was then applied to prepare porous membranes, which was the same as the swelling treatment of thin films deposited on silicon wafers.

2.5. Characterization

The chemical structures of PDMAEMA before and after CO_2 stimuli were measured by ^{1}H NMR spectroscopy (NMR, AV400, Bruker) using D_2O as the solvent. The zeta potential and size of PDMAEMA-*b*-PS micellar nanoparticles were examined by a laser granularity apparatus (Zetasizer Nano ZS ZEN3600). The surface potentials of PDMAEMA-*b*-PS membranes were determined by an electrokinetic analyzer (SurPASS Anton Paar, Austria). The surface and cross-sectional morphologies of all samples were tested using a field emission scanning electron microscope (FESEM, Hitachi S4800) and a thin gold layer was coated on the samples through ions sputtering to enhance conductivity before SEM observation. For cross-sectional morphologies observation, the samples were immersed into liquid nitrogen and quickly broken off to expose the cross sections. At least 100 pores of surface morphologies were measured to estimate the pore size distribution using the software *Nanomeasurer*. The static water contact angle (WCA) was recorded by a contact angle goniometer (Dropmeter A100, Maist) to evaluate the surface hydrophilicity of films. In addition, dynamic WCA was measured to estimate waterdrop infiltration process. For the WCA test of the membrane after CO_2 treatment, all samples were freeze-dried before testing to preserve the morphologies of surface and nanopores. The thickness and refractive index of dry films were determined using a spectroscopic ellipsometer (Complete EASE M − 2000U, J. A. Woollam) with an incident angle of 70°. For wet films, the sample stage of the spectroscopic ellipsometer was switched to liquid cell to record the thickness change of films in deionized water in situ. The frequency and dissipation shifts of the BCP films coated on Au sensors were recorded by a quartz crystal microbalance with dissipation (QCM-D, Q-Sense E400, Biolin) to estimate conformational transition of PDMAEMA chains.

2.6. Filtration tests

The separation performances of membranes were examined under vacuum pressure of 0.5 bar utilizing a dead-end filtration device with an effective diameter of 2 cm (Fig. S1). Before testing, vacuum pre-compression of each membrane was performed under 0.5 bar for 10 min to obtain a steady water permeance. The volume of water permeating through the membranes was recorded every 5 min, and the permeance (*Perm*) was calculated by Eq. (1):

$$Perm = \frac{V}{A \cdot t \cdot p} \quad (1)$$

where V (L) is the volume of water permeating through the membranes, A (m^2) is the active membrane area, t (h) is the filtering time, p (bar) is

the transmembrane pressure.

A variety of proteins including BSA, BHb, lysozyme and cytochrome *c* were used to conduct the rejection tests. The protein aqueous solutions were prepared with a concentration of 0.5 g/L. The protein concentrations in the feed and filtrate solutions were determined using a UV–vis absorption spectrometer (NanoDrop 2000C, Thermo Fisher). The protein rejection was determined by Eq. (2):

$$R = \frac{C_f - C_p}{C_f} \times 100\% \quad (2)$$

where C_f and C_p are the protein concentration (g/L) in the feed and filtrate solution, respectively.

Dextrans with different molecule weight (10, 40, 70 and 500 kDa) were all dissolved in deionized water for testing molecular weight cut off (MWCO) of membranes, and corresponding concentration of each dextran component was 2.5, 1, 1, 2 g/L, respectively. The concentrations of mixed dextrans in the feed and filtrate solution were determined using gel permeation chromatograph (1515 GPC, Waters), and the relationship between MWCO and the effective pore size of membranes was calculated by Eq. (3):

$$r = 0.33\, Mw^{0.46} \quad (3)$$

where M_w is the MWCO of dextran (Da), and r is the effective pore size (Å) of membranes.

3. Results and discussion

3.1. CO_2-responsive behavior

Before the fabrication of PDMAEMA-*b*-PS membranes, the CO_2-responsive behavior of this membrane-forming material was first investigated. To examine the transition in chemical structure of PDMAEMA upon CO_2/N_2 exposure, ^{1}H NMR characterization was conducted in D_2O. From Fig. 1a, we observed that the pristine signals of methyl protons adjacent to nitrogen (a) and methylene groups (b, c) were located at 2.2, 2.6 and 4.0 ppm, respectively [30]. Along with CO_2 bubbling in D_2O, the signals of corresponding protons were shift to left, the lower filed, and the new proton signals were relocated at 3.2, 3.6 and 4.4 ppm, respectively, which demonstrated the formation of quaternary amine as a result of the protonation of tertiary amine under the presence of bicarbonate. Then, N_2 served as the inert gas was further bubbled in the aqueous solution for a certain duration to remove CO_2. We observed that the proton signals of corresponding methyl and methylene was shifted to right again, indicating the reversible conversion of quaternary amine to tertiary amine. However, it should be note that the signal peaks related to methyl (a) and methylene (b) protons did not completely go back to the original positions after N_2 bubbling. This may be caused by the presence of partial quaternary amine groups, indicating that a small part of quaternary amine remained after the treatment of N_2.

To further investigate the conformation and charge transition of PDMAEMA chains in water under the alternative stimulation of CO_2/N_2, PDMAEMA-*b*-PS micelles with PDMAEMA as the shell and PS as the core were used, in which the chain dimension and charge state can be directly evaluated. As shown in Fig. S1, PDMAEMA-*b*-PS micelles exhibited a uniform spherical morphology, and the average diameter of the micelles in the dry state was determined to be 120 nm. The chain transition and charge state of the micelles were determined by the zeta potential and particle size measurement. As shown in Fig. 1b, PDMAEMA-*b*-PS micelles in water had a pristine average diameter of 135 nm, which is higher than the diameter in the dried state as measured by SEM. This is due to the water uptake and swelling of PDMAEMA chains in water. The diameter of micelles was rapidly increased to 180 nm after bubbling CO_2 for 6 min, and the zeta potential of the corresponding micelles was also increased from 49 to 71 mV because of the protonation of tertiary amine. After excluding CO_2 by bubbling N_2 in the solution, the micelle diameter was decreased to 128 nm and the zeta potential was decreased to 46 mV. Both values were lower than the pristine ones, which may be caused by the dissolution of traces of CO_2 from air in the micellar solution before the cyclic stimulation of CO_2/N_2, making PDMAEMA chains stretched and protonated slightly. By comparing the diameter of the micelles in the alternative exposure of CO_2/N_2, the thickness change of the PDMAEMA shell of the micelle induced by conformation transition upon CO_2/N_2 stimulation can be determined to be ~26 nm as the PS cores of the micelles remained unchanged during the CO_2/N_2 stimulation. Meanwhile, the change trend of zeta potential was highly synchronous with the change in micellar diameter. The conformation transition was mainly attributed to the electrostatic repulsion of charged PDMAEMA chains after CO_2 introduction [31]. After five cycles of CO_2/N_2 alternative exposure, the diameter of micelle can return to 130 nm and the corresponding zeta potential was also back to 48 mV, indicating that PDMAEMA chains exhibit good switchability and reversibility under the cyclic stimulation of CO_2/N_2.

3.2. Nanoporous PDMAEMA-b-PS thin films

On the basis of the strategy of selective swelling-induced pore generation, the PDMAEMA-*b*-PS dense films were obtained by spin-coating the BCP solution onto clean silicon wafers, and then immersed in ethanol at 65 °C for preset durations to produce nanoporous films. As shown in Fig. S3, the film before swelling showed a smooth and defect-free morphology. After swelling in hot ethanol for preset durations, nanoporous structures were observed clearly from the surface and cross-sectional SEM images (Fig. 2, Fig. S3, Fig. S4). As the films were

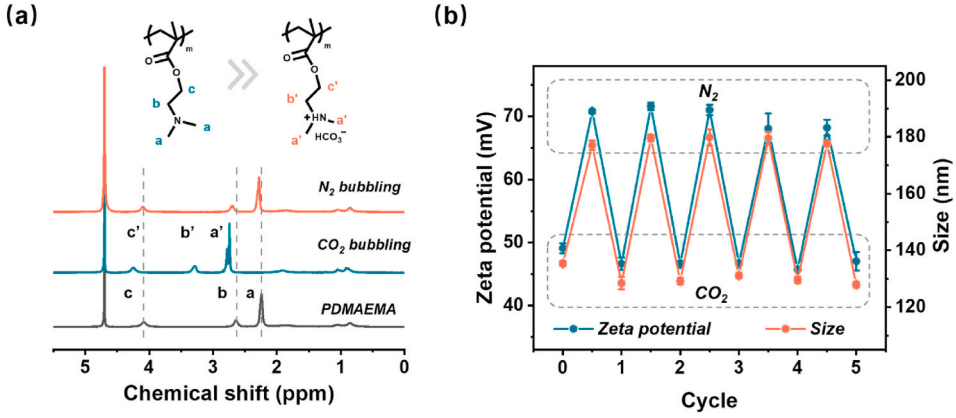

Fig. 1. (a) The chemical shifts of PDMAEMA after the alternative stimulation of CO_2/N_2. (b) Zeta potentials and sizes of PDMAEMA-*b*-PS micelles after the cyclic stimulation of CO_2/N_2.

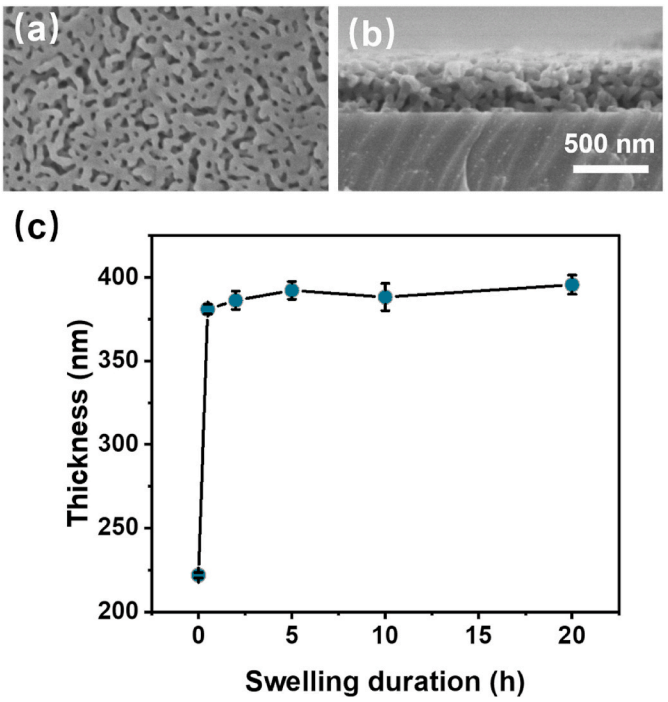

Fig. 2. The (a) surface and (b) cross-sectional SEM images of the PDMAEMA-*b*-PS films immersed in ethanol at 65 °C for 10 h. (c) The thicknesses of films for varied swelling durations. All images have the same scale bar as given in (b).

exposed in hot ethanol, ethanol molecules penetrated into films and enriched in the microdomains of PDMAEMA blocks. PDMAEMA phases were swollen, experienced volume expansion, and tended to connect with each other. After withdrawn the films from the ethanol to dry, the swollen PDMAEMA chains collapsed on the surface and pore walls, and the volumes previously occupied by the swollen PDMAEMA chains were converted to pores [32,33]. With the prolonged swelling, we first observed the isolated pores on the film surface, then the pores began to fuse to form elongated pores, finally the bi-continuous porous structure was formed (Fig. S3). Except for the change of pore morphology, the variation of film thicknesses is the key parameter to investigate the kinetics of selective swelling process, because the films only occur vertical expansion on confined substrates and the film porosity is associated with the thickness variation. As shown in Fig. 2c, the thickness of film showed a rapid increase after swelling in hot ethanol for 0.5 h, and the porosity was calculated to be 34%. When the swelling duration was increased from 2 h to 20 h, the thickness of films showed no obvious increase, indicating that the pores generation in whole films mainly occurred within the initial period of 0.5 h.

We monitored the thickness change of prepared nanoporous films in water upon CO_2 exposure by spectroscopic ellipsometry. The thickness of the pristine film prepared by swelling at 65 °C for 10 h was determined to be 387 nm in the dry state. As shown in Fig. 3, after the film was placed in the liquid cell filled with deionized water, the film thickness showed a stable thickness of 407 nm, which is thicker than the one of the dry film, because of the swelling and stretching of PDMAEMA chains enriched on the film surface in water. After replacing deionized water with CO_2-saturated water, the thickness soared to 424 nm once the film was placed in the liquid cell, then showed a rapid rise to 432 nm in the initial period of 20 min. The final thickness of the fillm reached ~436 nm as the immersing time lasted for 2 h, indicating that protonated PDMAEMA chains took a highly stretched conformation as a consequence of the effect of electrostatic repulsion. The total thickness increase caused by the CO_2 stimulation was determined to be 29 nm, which is approximate to the value measured from PDMAEMA-*b*-PS micelles.

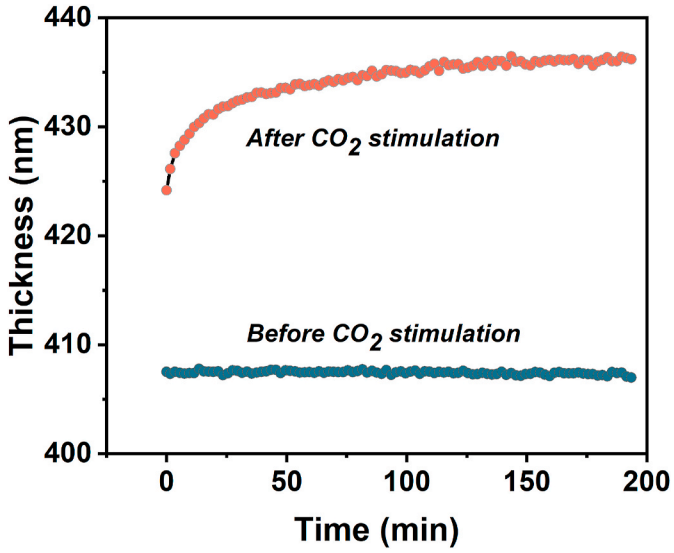

Fig. 3. The thickness change of nanoporous PDMAEMA-*b*-PS films before and after CO_2 stimulation.

In order to gain more understandings on conformation transition of PDMAEMA chains under the stimulation of CO_2, QCM-D was further utilized to determine the real-time responses of PDMAEMA chains. We prepared the testing sample by spin-coating the PDMAEMA-*b*-PS onto an Au chip and swelling in ethanol at 65 °C for 10 h. As shown in Fig. 4a, the initial data of the bare chip in contact with flowing deionized water with a flow rate of 80 μL/min served as baseline, and the frequency and dissipation shift remained constant at zero. Then the nanoporous PDMAEMA-*b*-PS film was first tested upon deionized water exposure. The frequency and dissipation at overtones of 5, 7 and 9 were collected to analyze the stiffness variation of the film, and the result showed the film exhibited a soft nature because of separated dissipation shift for different harmonics after reaching equilibrium. Subsequently, an obvious increase in dissipation and a drop in frequency were observed after switching deionized water to CO_2-saturated water, which demonstrated that the protonated PDMAEMA chains exhibit a softer trend presumably due to the stretched conformation transition [34]. After removing CO_2 by N_2 bubbling, the frequency and dissipation recovered to the initial states, manifesting that the property of the PDMAEMA-*b*-PS film prepared by selective swelling is reversible by CO_2/N_2 alternation. The smartfit model was fit to estimate the surface viscosity and elastic modulus of the film under CO_2 stimulation. As shown in Fig. 4b, the viscosity value of the film in deionized water was about 44 Pa·s. After introducing CO_2, the viscosity was rapidly decreased to 6 Pa·s. When bubbling inert N_2 to replace CO_2, the viscosity returned to the initial value. The change of elastic modulus (Fig. 4c) was similar to that of viscosity, that is, the film exhibited a higher elastic modulus while switched to a lower elastic modulus after CO_2 stimulation due to stretched conformation of PDMAEMA chains. Notably, the lower viscosity and the more flexible surface enable the film to have the potential of good anti-fouling ability [35].

Static and dynamic water contact angle (WCA) tests were performed to investigate the change of surface hydrophilicity before and after CO_2 stimulation. The static WCA of the PDMAEMA-*b*-PS film deposited on silicon wafers subjected to swelling at 65 °C for 10 h was determined to be 67.8°, indicating the film is relatively hydrophilic. After immersed in CO_2-saturated water for 12 h to adequately protonate the PDMAEMA chains, the film exhibited a WCA value of 61.1°, indicating that CO_2 exposure slightly improves the hydrophilicity of the PDMAEMA-*b*-PS film because of the protonation of the PDMAEMA chains enriched on the surface. The dynamic WCAs of PDMAEMA-*b*-PS membranes were further measured to investigate the surface wettability before and after

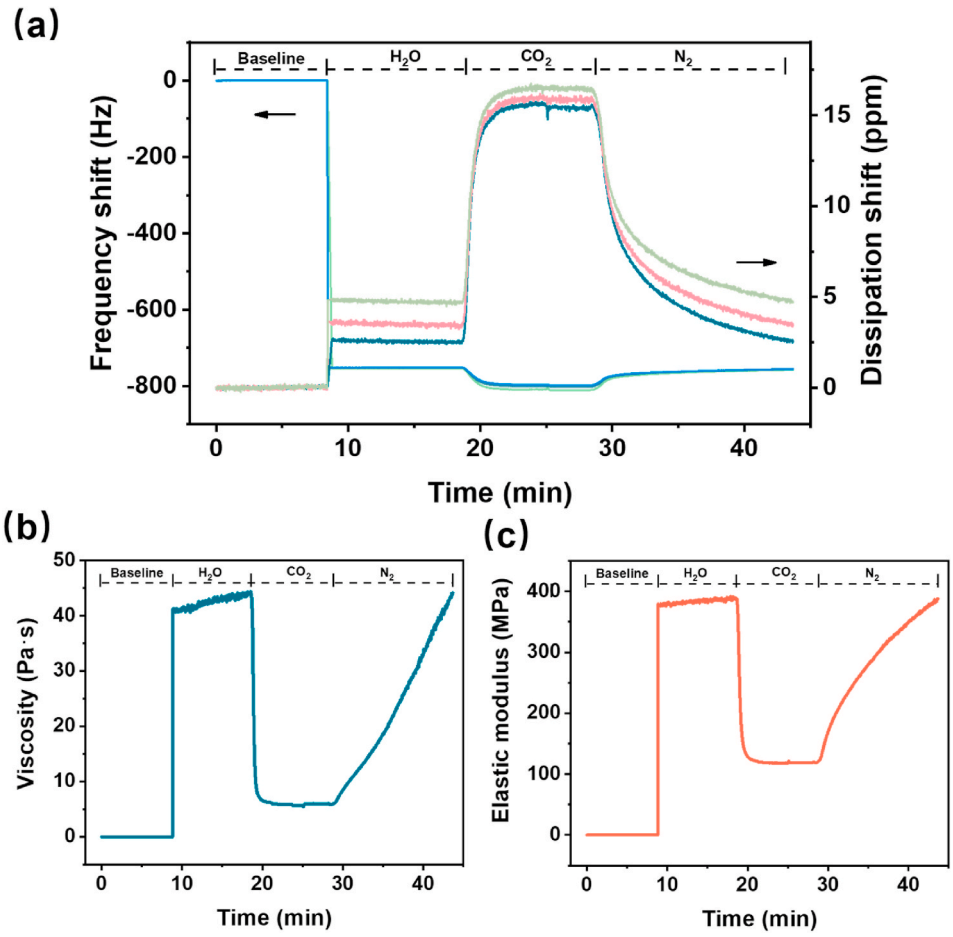

Fig. 4. (a) The frequency and dissipation responses of the nanoporous PDMAEMA-*b*-PS film with overtones of 5, 7, 9. The transition of (b) viscosity and (c) elastic modulus of the film under CO_2 stimulation.

CO_2 stimulation. As shown in Fig. 5, the WCA of the membrane before CO_2 stimulation was 71° at the beginning, subsequently a rapid decline of WCA occurred due to the spreading of water droplet on the membrane surface in the initial permeation state. Thereafter the WCA was decreased from 62° to 19° due to the downward permeation of water droplet within a short time of 28 s. In contrary, the membrane stimulated by CO_2 showed an initial WCA of 64° at the beginning, which is lower than the value of the membrane untreated. A relatively slow decline of WCA was observed in the process of downward permeation, as it took 140 s for the WCA to decrease from 62° to 15°. The WCA decline of the membrane stimulated by CO_2 exhibited a much smaller slope although it showed higher hydrophilicity than the membrane before CO_2 stimulation. This revealed the pores of the membrane became narrow slowing down the permeation of water droplet, because the protonated PDMAEMA stretched to form the thicker layer. It is in good agreement with the result of spectroscopic ellipsometry discussed above.

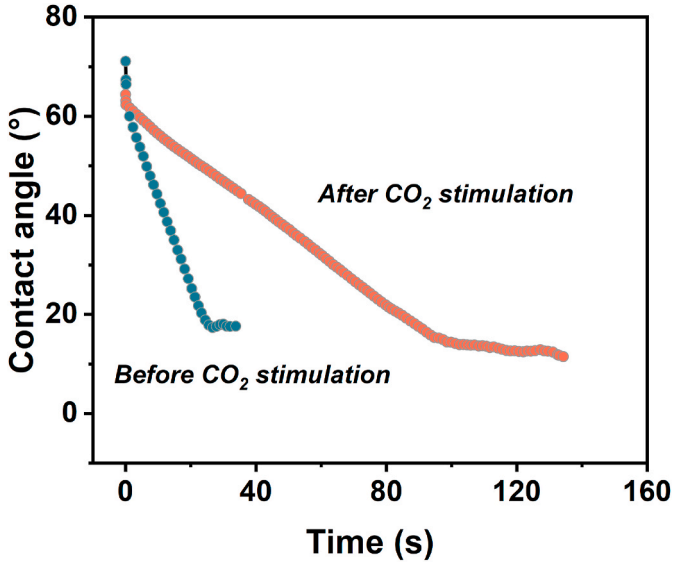

Fig. 5. Dynamic WCAs of PDMAEMA-*b*-PS membranes before and after CO_2 stimulation.

3.3. Separation performances

After confirming the variation of zeta potential and chain conformation under the alternant stimulation of CO_2/N_2, the PDMAEMA-*b*-PS membranes were prepared to investigate the separation performances. The water permeances of membranes showed a significant increase with prolongated swelling durations as shown in Fig. 6a. When the swelling duration was 0.5 h, the permeance of membrane was 397 $L{\cdot}h^{-1}{\cdot}m^{-2}{\cdot}bar^{-1}$ upon N_2 exposure. With the duration prolongated to 2 h, the permeance was increased to 477 $L{\cdot}h^{-1}{\cdot}m^{-2}{\cdot}bar^{-1}$. After swelling for 5 h, the membranes showed a gradual increase to 778 $L{\cdot}h^{-1}{\cdot}m^{-2}{\cdot}bar^{-1}$. As the duration was further extended from 10 h to 20 h, the permeance exhibited a slow growth, rising from 1080 to 1126 $L{\cdot}h^{-1}{\cdot}m^{-2}{\cdot}bar^{-1}$. There are two reasons for the enhancing of permeances with prolongated durations: one is from the enlarged pore size

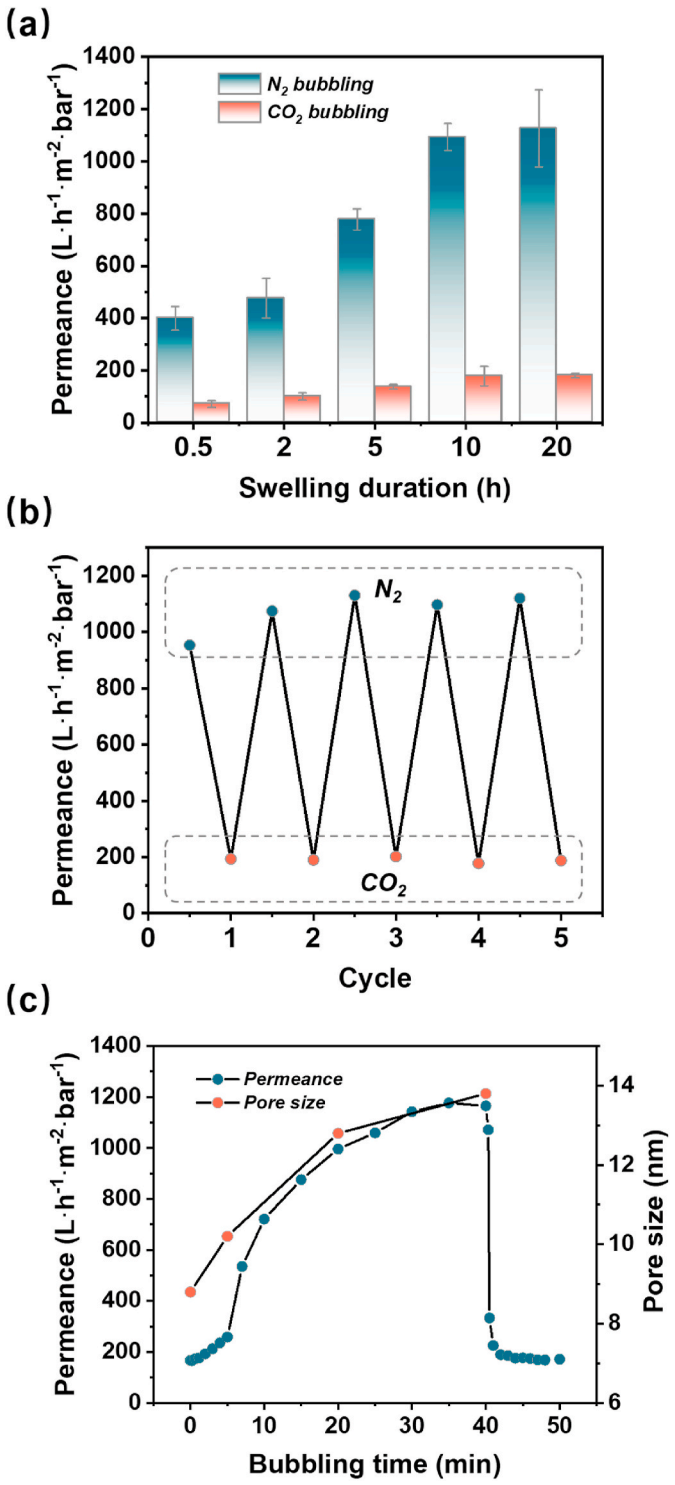

Fig. 6. (a) The permeances of PDMAEMA-*b*-PS membranes prepared by swelling at 65 °C for varied swelling durations under CO_2/N_2 stimulation. (b) The permeance switchability of membranes prepared by swelling at 65 °C for 10 h. (c) The permeances and corresponding pore sizes of the membrane for varied N_2 bubbling time.

of the membrane; the other is from the enrichment of hydrophilic PDMAEMA chains on the membrane surface and pore walls [36]. After bubbling CO_2 into water, the permeance of membrane was declined greatly. There still existed the trend that the longer the swelling duration, the higher the permeance. For 0.5 h swelling, the membrane showed a much lower permeance of 72 $L{\cdot}h^{-1}{\cdot}m^{-2}{\cdot}bar^{-1}$ under CO_2 stimulation, indicating that the protonated PDMAEMA chains blocked the pores. The difference in permeances by N_2/CO_2 alternation was 327 $L{\cdot}{\cdot}h^{-1}{\cdot}m^{-2}{\cdot}bar^{-1}$. Further extending duration to 2 h, the permeance was 100 $L{\cdot}h^{-1}{\cdot}m^{-2}{\cdot}bar^{-1}$ after CO_2 bubbling, and the permeance difference was 377 $L{\cdot}h^{-1}{\cdot}m^{-2}{\cdot}bar^{-1}$. As the swelling duration was further extended to 5, 10, 20 h. The difference values of permeances under the stimulation of CO_2/N_2 was 641, 902, 950 $L{\cdot}h^{-1}{\cdot}m^{-2}{\cdot}bar^{-1}$, respectively. These results demonstrate that CO_2/N_2 transition enables the effective regulation of the membrane permeances.

The cyclic tests of water permeances under CO_2/N_2 alternative stimulation were further conducted to investigate the reversibility of membrane performances. The membrane subjected to swelling at 65 °C for 10 h was chosen for the cyclic tests. As shown in Fig. 6b, the pristine permeance of membrane was 950 $L{\cdot}h^{-1}{\cdot}m^{-2}{\cdot}bar^{-1}$. After CO_2 bubbling into deionized water, the permeance was rapidly decreased to 185 $L{\cdot}h^{-1}{\cdot}m^{-2}{\cdot}bar^{-1}$ due to the expansion of protonated PDMAEMA chains. Subsequently, N_2 served as the inert gas was introduced to remove CO_2, and the permeance of membrane was increased to 1130 $L{\cdot}h^{-1}{\cdot}m^{-2}{\cdot}bar^{-1}$ in the first cycle. After the fifth cycle, the permeance could still return to 1180 $L{\cdot}h^{-1}{\cdot}m^{-2}{\cdot}bar^{-1}$, confirming that the reversibility in permeance switching can be realized under CO_2/N_2 stimulation.

To determine the effective pore size change of the membrane upon stimulation, the MWCOs were determined by testing the membrane rejections to dextrans with varied molecules weights, and corresponding effective pore sizes were calculated according to Eq. (3) [37]. As shown in Fig. 6c, the membrane prepared by swelling at 65 °C for 10 h showed a permeance of 186 $L{\cdot}h^{-1}{\cdot}m^{-2}{\cdot}bar^{-1}$ under CO_2 stimulation. Correspondingly, MWCO was measured to be 43 kDa (Fig. S6), and the effective pore size was about 8.8 nm. With N_2 bubbling to remove CO_2, both the permeance and MWCO exhibited a gradual rise. After N_2 bubbling for 5 min, the membrane showed the permeance of 580 $L{\cdot}h^{-1}{\cdot}m^{-2}{\cdot}bar^{-1}$ and a MWCO of 59 kDa, and pore size grew to 10.4 nm. Further extending N_2 stimulated time to 20 min, the permeance of membrane returned to 1060 $L{\cdot}h^{-1}{\cdot}m^{-2}{\cdot}bar^{-1}$, correspondingly the MWCO was also increased to 93 kDa. While the bubbling time was over 30 min, no significant change of the permeance was observed, remaining stable at 1165 $L{\cdot}h^{-1}{\cdot}m^{-2}{\cdot}bar^{-1}$. The MWCO was determined to be 110 kDa, and the corresponding pore size was increased from 12.8 nm to 13.9 nm because of the conformation change of PDMAEMA chains under N_2 stimulation.

As is well known, the permeance of membrane was not only determined by the pore size but also the membrane thickness. Therefore, we introduced classic Hagen-Poiseuille equation to fit experiment data (Eq. S(1)). Moreover, the film showed relatively narrow pore size distribution (Fig. S5), which benefits from the microphase separation nature of BCP-based films and the selective swelling pore generation strategy. The average pore size of membrane was obtained from the MWCO tests, and the membrane thickness was determined by spectroscopic ellipsometry with liquid cell. Inputting the measured data into Hagen-Poiseuille equation, the calculated data of the membrane permeance under N_2 stimulation is 6.9 times higher than the permeance after CO_2 introduction. The actual data we tested in the experiment was about 5 times. Considering the flow regime difference and tortuosity change are inevitable in the practical operation resulting in the variation of correction factor K (Eq. S(2)) [38,39], the difference between theoretical and calculated values is reasonable.

Moreover, the rejections of PDMAEMA-*b*-PS membranes to proteins with varied sizes and charge properties including BSA, BHb, lysozyme and cytochrome *c* were shown in Fig. 7. Obviously, a higher rejection to each protein was obtained under CO_2 stimulation, as a contrast, removing CO_2 could result in a low rejection correspondingly. The BSA rejection of 91.5% and BHb rejection of 89.1% were realized in the presence of CO_2. After removing CO_2 in water, the BSA and BHb rejections were decreased to 15.8% and 21.9%, respectively. As discussed above, the MWCO of the membrane is 43 kDa in the existence of CO_2, which is lower than the molecular weight of BSA and BHb. In addition,

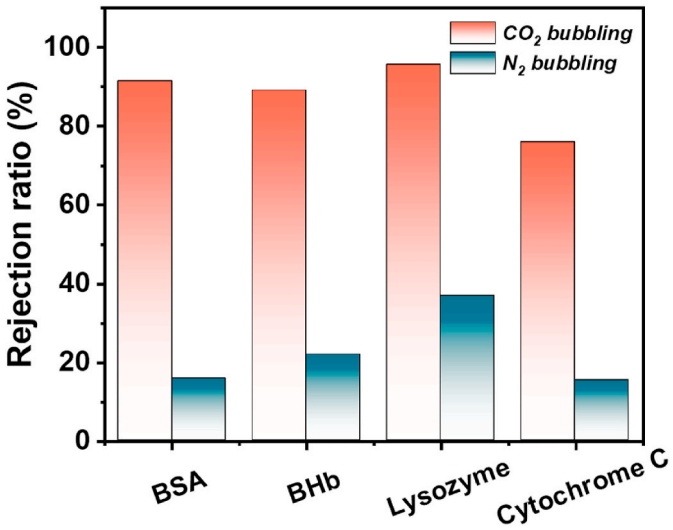

Fig. 7. The rejections of the PDMAEMA-*b*-PS membrane to different proteins.

the isoelectric points of BSA and BHb are 4.7 and 7.0, respectively [40]. Considering the surface zeta potential of membrane (Fig. S7), there should be no obvious electrostatic repulsion between the membrane and BSA or BHb, so we conclude that the high rejection to BSA and BHb mainly depends on size sieving. Furthermore, we also observed the high rejections to lysozyme and cytochrome *c* (95.6% and 75.9%) in the presence of CO_2, while their molecular weights are lower than the MWCO of membrane. The isoelectric points of lysozyme and cytochrome *c* are 11.3 and 9.8 [41,42], respectively, indicating both of them showed positive charge. Considering the membrane was positively charged under CO_2 stimulation, the rejection to the positively charged proteins of lysozyme and cytochrome *c* could be attributed to electrostatic repulsion. More spectrum details of different proteins rejections under CO_2/N_2 stimulation are given in Fig. S8.

4. Conclusions

In this work, by using the strategy of selective swelling-induced pore generation, we developed the CO_2-responsive PDMAEMA-*b*-PS membranes that enable to reversibly regulate separation performances. We first demonstrated the reversible transition in chemical structure of PDMAEMA, as well as the conformation and charge transition of PDMAEMA-*b*-PS upon CO_2/N_2 alternation. Then, spectroscopic ellipsometry was further utilized to monitor the real-time responses of PDMAEMA-*b*-PS films upon CO_2 exposure. The results manifested the thickness change caused by the stretching of protonated PDMAEMA chains in CO_2-saturated water, which also led to the pore size change films. QCM-D measurement gave more insight into the surface viscosity and elastic modulus change of the film under the CO_2 stimulation. Based on these properties, the PDMAEMA-*b*-PS membranes were utilized to evaluate the separation performances. The permeance could be facilely regulated by CO_2/N_2 stimulation as well as changing the swelling durations. The membranes exhibited good reversible switching in permeance after manifold cycles of CO_2/N_2 alternation. Moreover, the rejection tests showed the membranes were competent for varied proteins rejection based on different separation principles. This study provides a simple and reliable way of selective swelling-induced pore generation to prepare CO_2-responsive membranes, and demonstrates the great potential for separation applications.

Author statement

Chenxu Zhang: Investigation, Data curation, Writing-orginal draft preparation.
Xiangyue Ye: Investigation
Zhuo Li: Validation.
Jiemei Zhou: Methodology, Writing-review & editing.
Yong Wang: Conceptualization, Supervision.
All authors have approved to the final version of the manuscript.

Declaration of competing interest

The authors declare that they have no known competing financial interests or personal relationships that could have appeared to influence the work reported in this paper.

Acknowledgments

Financial support from the National Natural Science Foundations of China (21908095), and the Natural Science Foundation of Jiangsu Province (BK20190671) is gratefully acknowledged.

Appendix A. Supplementary data

Supplementary data related to this article can be found at https://doi.org/10.1016/j.memsci.2021.119928.

References

[1] M.A. Shannon, P.W. Bohn, M. Elimelech, J.G. Georgiadis, B.J. Marinas, A. M. Mayes, Science and technology for water purification in the coming decades, Nature 452 (2008) 301–310.
[2] A. Lee, J.W. Elam, S.B. Darling, Membrane materials for water purification: design, development, and application, Environ. Sci.: Water Res. Technol. 2 (2016) 17–42.
[3] N. Hampu, J.R. Werber, W.Y. Chan, E.C. Feinberg, M.A. Hillmyer, Next-generation ultrafiltration membranes enabled by block polymers, ACS Nano 14 (2020) 16446–16471.
[4] S.B. Darling, Perspective: interfacial materials at the interface of energy and water, J. Appl. Physiol. 124 (2018), 030901.
[5] Z. Liu, W. Wang, R. Xie, X.J. Ju, L.Y. Chu, Stimuli-responsive smart gating membranes, Chem. Soc. Rev. 45 (2016) 460–474.
[6] D. Wandera, S.R. Wickramasinghe, S.M. Husson, Stimuli-responsive membranes, J. Membr. Sci. 357 (2010) 6–35.
[7] M.L. Chen, M.D. Dong, R. Havelund, V.R. Regina, R.L. Meyer, F. Besenbacher, P. Kingshott, Thermo-responsive core-sheath electrospun nanofibers from poly (N-isopropylacrylamide)/Polycaprolactone blends, Chem. Mater. 22 (2010) 4214–4221.
[8] Y. Zhao, Light-responsive block copolymer micelles, Macromolecules 45 (2012) 3647–3657.
[9] L.N. Zhang, A. Ghaffar, X.Y. Zhu, B.L. Chen, Stable graphene-based membrane with pH-responsive gates for advanced molecular separation, Environ. Sci. Technol. 53 (2019) 10398–10407.
[10] M. Sakurai, Y. Kobori, T. Tachikawa, Structural dynamics of lipid bilayer membranes explored by magnetic field effect based fluorescence microscopy, J. Phys. Chem. B 123 (2019) 10896–10902.
[11] T. Xiang, T. Lu, W.F. Zhao, C.S. Zhao, Ionic-strength responsive zwitterionic copolymer hydrogels with tunable swelling and adsorption behaviors, Langmuir 35 (2019) 1146–1155.
[12] Y.Z. Li, L.Q. Zhu, N. Grishkewich, K.C. Tam, J.Y. Yuan, Z.P. Mao, X.F. Sui, CO_2-Responsive cellulose nanofibers aerogels for switchable oil-water separation, ACS Appl. Mater. Interfaces 11 (2019) 9367–9373.
[13] Q. Zhang, Z.W. Wang, L. Lei, J. Tang, J.L. Wang, S.P. Zhu, CO_2-Switchable membranes prepared by immobilization of CO_2-breathing microgels, ACS Appl. Mater. Interfaces 9 (2017) 44146–44151.
[14] L.L. Dong, Y. Zhao, CO_2-switchable membranes: structures, functions, and separation applications in aqueous medium, J. Mater. Chem. 8 (2020) 16738–16746.
[15] H.L. Che, M. Huo, L. Peng, T. Fang, N. Liu, L. Feng, Y. Wei, J.Y. Yuan, CO_2-Responsive nanofibrous membranes with switchable oil/water wettability, Angew. Chem. Int. Ed. 54 (2015) 8934–8938.
[16] L.L. Dong, W.Z. Fan, H.J. Zhang, M.Q. Chen, Y. Zhao, CO_2-Responsive polymer membranes with gas-tunable pore size, Chem. Commun. 53 (2017) 9574–9577.
[17] K.A.S. Bornillo, S. Kim, H. Choi, Cu (II) removal using electrospun dual-responsive polyethersulfone-poly (dimethyl amino) ethyl methacrylate (PES-PDMAEMA) blend nanofibers, Chemosphere 242 (2020) 125287.
[18] S. Wohlhauser, G. Delepierre, M. Labet, G. Morandi, W. Thielemans, C. Weder, J. O. Zoppe, Grafting polymers from cellulose nanocrystals: synthesis, properties, and applications, Macromolecules 51 (2018) 6157–6189.
[[19]] J.J. Li, Y.N. Zhou, Z.H. Luo, Mussel-inspired V-shaped copolymer coating for intelligent oil/water separation, Chem. Eng. J. 322 (2017) 693–701.

[20] S. Hemmila, J.V. Cauich-Rodriguez, J. Kreutzer, P. Kallio, Rapid, simple, and cost-effective treatments to achieve long-term hydrophilic PDMS surfaces, Appl. Surf. Sci. 258 (2012) 9864–9875.
[21] D. Rana, T. Matsuura, Surface modifications for antifouling membranes, Chem. Rev. 110 (2010) 2448–2471.
[22] Y. Wang, Nondestructive creation of ordered nanopores by selective swelling of block copolymers: toward homoporous membranes, Acc. Chem. Res. 49 (2016) 1401–1408.
[23] X.S. Shi, Z. Xu, C.B. Huang, Y. Wang, Z.F. Cui, Selective swelling of electrospun block copolymers: from perforated nanofibers to high flux and responsive ultrafiltration membranes, Macromolecules 51 (2018) 2283–2292.
[24] Z.G. Wang, Y. Wang, Highly permeable and robust responsive nanoporous membranes by selective swelling of triblock terpolymers with a rubbery block, Macromolecules 49 (2016) 182–191.
[25] Z.G. Wang, L.M. Guo, Y. Wang, Isoporous membranes with gradient porosity by selective swelling of UV-crosslinked block copolymers, J. Membr. Sci. 476 (2015) 449–456.
[26] W. Sun, Z.G. Wang, X.P. Yao, L.M. Guo, X.Q. Chen, Y. Wang, Surface-active isoporous membranes nondestructively derived from perpendicularly aligned block copolymers for size-selective separation, J. Membr. Sci. 466 (2014) 229–237.
[27] F.G. Santos, L.C. Bonkovoski, F.P. Garcia, T.S.P. Cellet, M.A. Witt, C.V. Nakamura, A.F. Rubira, E.C. Muniz, Antibacterial performance of a PCL-PDMAEMA blend nanofiber-based scaffold enhanced with immobilized silver nanoparticles, ACS Appl. Mater. Interfaces 9 (2017) 9304–9314.
[28] M.F. Cunningham, P.G. Jessop, Carbon dioxide-switchable polymers: where are the future opportunities? Macromolecules 52 (2019) 6801–6816.
[29] J.M. Zhou, C.X. Zhang, Y. Wang, Nanoporous block copolymer membranes immobilized with gold nanoparticles for continuous flow catalysis, Polym. Chem. 10 (2019) 1642–1649.
[30] Y.B. Wei, Q. Zeng, J.Z. Huang, X.R. Guo, L.L. Wang, L.S. Wang, Preparation of gas-responsive imprinting hydrogel and their gas-driven switchable affinity for target protein recognition, ACS Appl. Mater. Interfaces 12 (2020) 24363–24369.
[31] X.Y. Li, R. Xie, Z.H. Jia, X.J. Ju, W. Wang, Z. Liu, L.Y. Chu, CO_2-Responsive poly(N, N-dimethylaminoethyl methacrylate) hydrogels with fast responsive rate, J. Taiwan Inst. Chem. Eng. 94 (2019) 135–142.
[32] N. Yan, Z.G. Wang, Y. Wang, Highly permeable membranes enabled by film formation of block copolymers on water surface, J. Membr. Sci. 568 (2018) 40–46.
[33] Z.G. Wang, R. Liu, Q.Q. Lan, Y. Wang, Selective swelling blends of block copolymers for nanoporous membranes with enhanced permeability and robustness, J. Polym. Sci., Part B: Polym. Phys. 55 (2017) 1617–1625.
[34] A.D. Easley, T. Ma, C.I. Eneh, J. Yun, R.M. Thakur, J.L. Lutkenhaus, A practical guide to quartz crystal microbalance with dissipation monitoring of thin polymer films, J. Polym. Sci. (2021), https://doi.org/10.1002/pol.20210324.
[35] G. Galli, E. Martinelli, Amphiphilic polymer platforms: surface engineering of films for marine antibiofouling, Macromol. Rapid Commun. 38 (2017) 1600704.
[36] Y.J. Wang, C.X. Zhang, J.M. Zhou, Y. Wang, Room-temperature swelling of block copolymers for nanoporous membranes with well-defined porosities, J. Membr. Sci. 608 (2020) 118186.
[37] J.I. Calvo, R.I. Peinador, P. Pradanos, L. Palacio, A. Bottino, G. Capannelli, A. Hernandez, Liquid-liquid displacement porometry to estimate the molecular weight cut-ff of ultrafiltration membranes, Desalination 268 (2011) 174–181.
[38] J.C. Cai, E. Perfect, C.L. Cheng, X.Y. Hu, Generalized modeling of spontaneous imbibition based on hagen-Poiseuille flow in tortuous capillaries with variably shaped apertures, Langmuir 30 (2014) 5142–5151.
[39] R.Z. Waldman, F. Gao, W.A. Phillip, S.B. Darling, Maximizing selectivity: an analysis of isoporous membranes, J. Membr. Sci. 633 (2021), 119389.
[40] X.Y. Qiu, H.Z. Yu, M. Karunakaran, N. Pradeep, S.P. Nunes, K.V. Peinemann, Selective separation of similarly sized proteins with tunable nanoporous block copolymer membranes, ACS Nano 7 (2013) 768–776.
[41] A. Vinu, V. Murugesan, O. Tangermann, M. Hartmann, Adsorption of cytochrome c on mesoporous molecular sieves: influence of pH, pore diameter, and aluminum incorporation, Chem. Mater. 16 (2004) 3056–3065.
[42] M.M. Lynch, J.C. Liu, M. Nigra, M.O. Coppens, Chaperonin-Inspired pH protection by mesoporous silica SBA-15 on myoglobin and lysozyme, Langmuir 32 (2016) 9604–9610.